

## **Increased Spatial Resolution with a Single Nozzle in Fused Filament Fabrication Through Controlled Distributions and Volume Fractions of Soluble and Insoluble Materials Including Formation of Functionally Graded Lattices**

I. A. Rybak\*, J. W. McKee†, J. T. Green‡

\*Department of Computer Science

†Department of Aerospace and Mechanical Engineering

‡Department of Engineering Education and Leadership  
The University of Texas at El Paso, El Paso, TX, 79902

### **Abstract**

Extrusion height and width are characteristic limits of spatial resolution in fused filament fabrication which are inextricably linked to nozzle diameter. Unlike structure size which is constrained by nozzle diameter and print stability, void dimensions may be controlled through the relative spacing of neighboring extrusions. To print features using a single nozzle with increased resolution as compared to conventional print methods, soluble support material was co-extruded with insoluble material in a multi-inlet active-mixing hotend including proportional mixing rod rotation. The ratio of materials and their rotational distributions within each extrusions were controlled in situ. Specimens were printed with connecting extrusions and support material was removed during post-processing to produce features smaller than the extrusion size. The versatility of this technique is demonstrated through microstructural control and the fabrication of functionally graded lattice systems using multiple inlets and variable volume fractions of materials and relative mixing rod rotation.

### **Introduction**

Lattice structures have long been a staple of structural optimization, given their high performance to weight ratio, with the intended application determining the style of lattice, its relative density, and method of lattice fabrication. Additive manufacturing (AM) is a preferred method in the production of complex structures due to the unique control and the capabilities available through multiple processes [1]. In final use cases, some influencing factors that would drive the use of AM may include the need for an internal structure that cannot be formed through subtractive manufacture, the benefit of rapid iteration time, or the desire for more complex functionality through the actual creation processes like temperature control, multi material production, and even the orientation of features [2], [3]. These structures can then be tested, often in compression, to measure their relative performance and determine the optimal properties of the whole structure under desired load conditions [4], [5]. Expanding this understanding leads to the development of different models and representations for lattice systems made through AM, many of which consider the basic unit cell that makes up the repeating structure [6], [7], [8], [9], [10]. Some investigations involve adapting the lattice structure to the intended geometry to achieve better manufacturing parameters and resultant performance [2], [11], [12], [13]. Of great

interest is micro-lattices, which apply benefits from lattices at a smaller scale which is helpful for additional functionalities such as heat transfer or porous designs [14].

Lattice structures may also incorporate elements of functionally graded structures by variation of their features. Functional grading allows for improved bioinspired applications of AM [15] and may be achieved through a number of different technological and design processes for a given use case or type of gradient [16]. Of particular interest here is the idea of a porosity gradient achieved on a micro-lattice scale by variation of the beam width and lengths.

A major deciding factor of what features may be produced through AM is the actual size of any printed feature, which generally cannot be smaller than the dimensions of the apparatus which produces that feature. In the case of fused filament fabrication (FFF), a technique becoming widely adopted for its low cost of implementation relative to the capabilities it offers, that dimension would be tied to the size of the printed extrusions which are limited by the diameter of the nozzle of the toolhead. In order to achieve high detail in a printed structure, a smaller nozzle diameter is conventionally required [17]. However, this increased feature resolution sacrifices print time as restricted flow through the toolhead reduces maximum extrusion size and more toolpaths are required to achieve an equivalent output volume. Additionally, the build orientation now plays an important role in the lattice design by restricting the lattice beam dimensions in the vertical direction and causing lower layer adhesion [18]. Furthermore, the spacing between beams is determined by the print pattern and location of the extrusions, as shown in **Figure 1A** and **1B**.

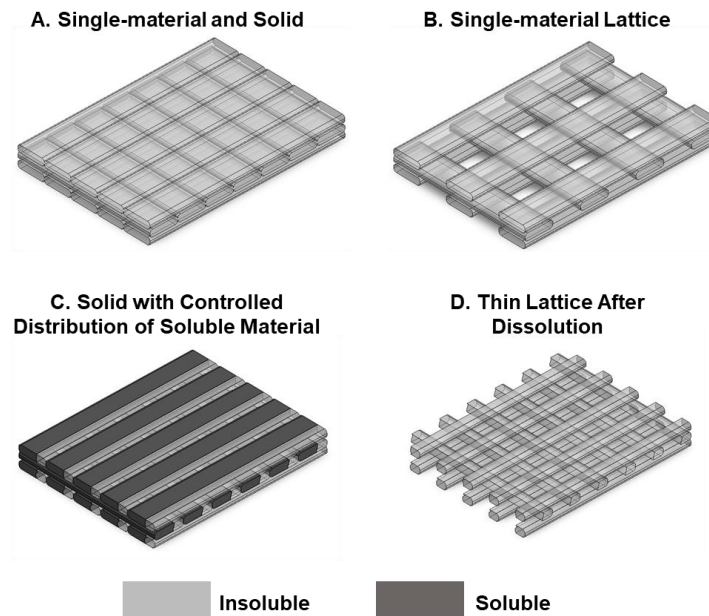


**Figure 1** – Demonstration of potential methods to achieve a lattice structure through fused filament fabrication

Research heavily explores what materials may be extruded through FFF printing. Multiple toolheads allow for switching materials during the printing process, which may also be achieved through user intervention. In addition, this offers the use of multiple nozzle diameters for different levels of detail or for materials with certain requirements like abrasive resistant

nozzle coatings or a minimum diameter to allow for composite flow such as chopped carbon fibers. Single nozzle systems have been developed which combine multiple inputs into a single outlet to achieve multi material production, often enabling functional gradients through controlled proportions of the different material flows during the print, called local composition control (LCC) [19], [20]. Additionally, methods exist to produce multi material extrusions through custom printhead designs for specific geometries [21]. Previously, a special active-mixing hotend which is capable of *in situ* control of multiple material flows and blend rates was used to investigate the potential for sub-extrusion scale LCC by limiting the rate of mixing in order to create distinct regions within each printed extrusion, demonstrated through printing of pigmented polylactic acid (PLA) filaments [22] as coatings which could theoretically be used as a method to improve surface finish of parts [23], [24].

This study expands on this work by producing beam lattices through coextrusion of PLA with a soluble material demonstrated in **Figure 1C** that is removed during post-processing to create a negative volume and leave the PLA as beams with sizes smaller than the original extrusions, as shown in **Figure 1D**. This investigation seeks to answer the following hypotheses through experimentation:

1. Selection of input flow direction and proportional rod rotation enable printing of extrusions with similar features even at perpendicular print directions
2. Post processing of printed structures sufficiently removes soluble material from a repeated lattice structure
3. Variation of volume fraction between coextruded materials allows for the creation of functionally graded lattices which perform differently to uniform lattice structures under tensile load

## **Methods**

### **Printer and material configuration**

In this study the active filament-mixing fabrication (AFMF) printer described in [19] was used with a 0.6mm diameter nozzle. Specimens printed for optical testing were printed with a pigmented Midnight Blue PRO series PLA (MatterHackers, CA, United States of America) and a generic white pigmented PLA. Specimens that were mechanically tested were printed with the same blue pigmented PLA and spoolWorks Scaffold soluble support filament (E3D-Online Limited, Oxfordshire, UK) which is a polyvinyl alcohol-based filament. The combination of these materials was chosen because of the wide availability of PLA filaments and past successes coextruding it with the scaffold material [25]. The AFMF printer has 3 available inlets, oriented at +90, -30, and -150° from the +X axis of the printer. The soluble filament was inserted into the inlet located +90° and the PLA filament was inserted into the remaining two inlets, which must always have a filament to prevent backflow.

### **Specimen design**

The basic unit cell investigated in this study is like that found in [26], which uses extrusions to form a cell that spans two layers with the extrusions themselves forming beams. While the beams could be at any angle to each other within the cell, printing a square shape

requires the most difference between extrusion directions and would serve to better demonstrate the use of mixing parameters to achieve extrusions with similar distribution of materials despite the printing direction.

To enable printing of the lattice design through multiple layers of the build direction and provide the necessary volume to achieve steady flow through the hotend following a change in print direction or mixing parameters such as volume fraction of materials, rod rotation ratio, and inlet, a rectangular print pattern with alternating concentric infill was created using PrusaSlicer 2.8.1 (Prusa Research, Prague, Czech Republic) and modified to support mixing commands in the Marlin firmware (marlinfw.org). This design, shown in **Figure 2**, was printed with an extrusion height of 0.2mm, width of 0.8mm, and 10 total layers with 5 in each primary direction. Printing speed was set to a constant 20mm/s. This lattice was then cut into a strip at 45° to orient the beams +/- 45° to a tensile load direction with the center of the concentric pattern making up a region of interest. A subset of this region of interest is the test region, which is placed between the grips during tensile testing. The additional volume of this print is necessary to ensure steady flow from the nozzle at the region of interest by providing sufficient extrusion after changing mix parameters or direction of nozzle movement. Each matching pair of concentric extrusions in the region of interest could be individually assigned mixing parameters.

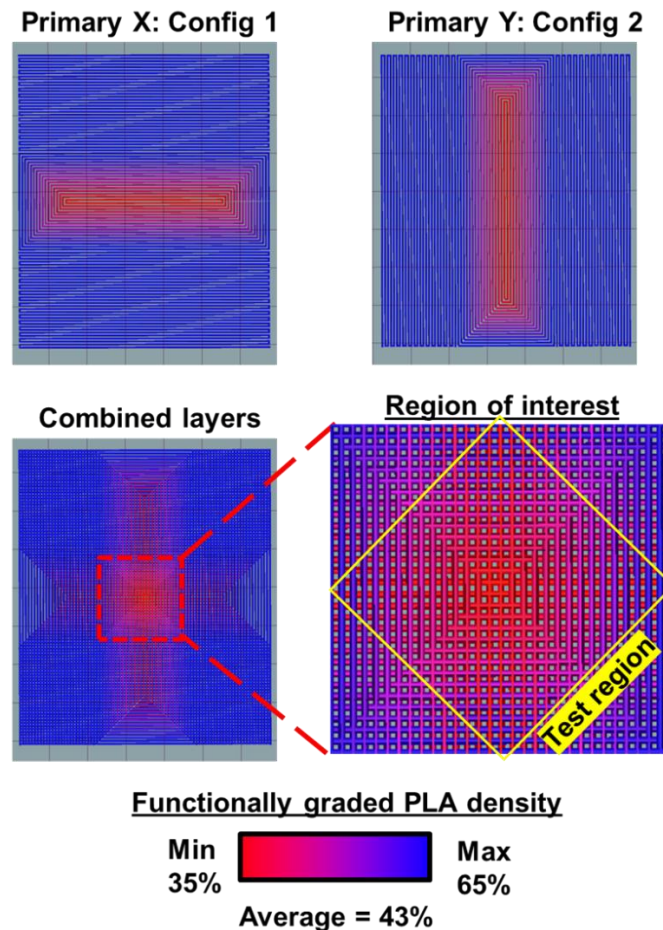


**Figure 2** – Print design pattern to produce uniform and functionally graded lattices using extrusions printed perpendicular to one another and then processing to a test region in the center.

Tensile tests were conducted to be able to compare a solid structure to a lattice. Though compression testing is common for lattice characterization, it is less effective to test a solid printed specimen. Additionally, the build direction of the print plays a reduced role in these tests as the test does not pull layers apart, but rather extrusions within a layer. Many studies have examined the orientation of these extrusions and the result on the test data [27] and a +/- 45° layup pattern for the beams relative to the pull direction was selected for mechanical tests. The test section for these specimens, a 1” square area, is contained within the larger region of interest so that functionally graded design could be implemented for each extrusion pair.

In order to facilitate micro-computed tomography (uCT) characterization of this technique, a specimen was designed and printed with an intentionally larger gap between the center-most extrusions to visually separate the direction of printing. This specimen was additionally processed down to a smaller size with fewer extrusions to ensure thorough removal of scaffold material during post-processing and fit in the uCT x-ray scanner. These specimens were not cut at the 45° angle but rather in a square design.

### **Mixing parameter selection**

To facilitate the lattice structure connecting multiple layers and forming the beam structure, mixing parameters needed to be selected for each primary print direction which ensured that PLA material would be present from the top to the bottom of the extrusion thereby facilitating connections between layers after soluble material is removed.

Tests to determine these mixing parameters were performed by printing large circles on the print bed with the white pigmented PLA representing “soluble” and the blue pigmented PLA as it would be in a final print. A 20% PLA to 80% soluble ratio was used in these tests to highlight the minimal structure of the PLA in the scaffold. Two different inlets were used for the PLA and swapped between, predicting that changing the physical entry point for the filament would assist in changing the distribution in the extrusion. These large multilayer circles were printed without any mixing rod rotation to establish a baseline for each of the inlet configurations. Cross sections of these circles are shown in **Figure 3** after sanding. From this, it was clear that even though the physical input location changed, the output location did not largely change, and the use of a mixing rod would be required for at least one of the configurations.

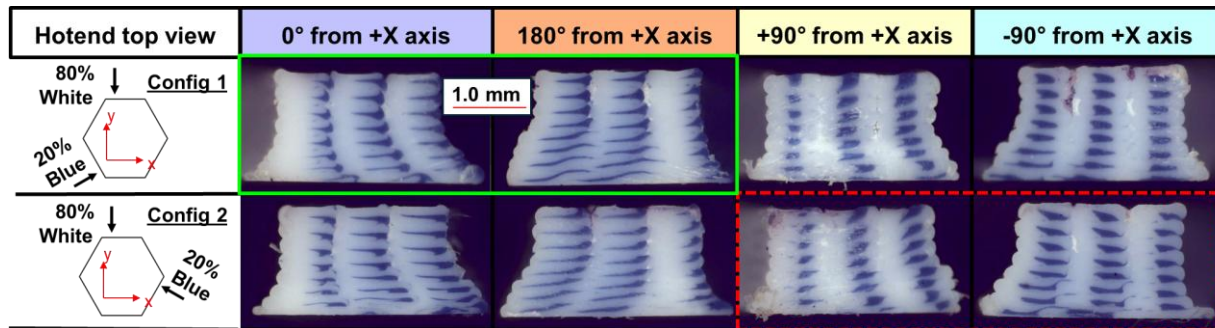


**Figure 3** – Cross sections of tests to determine baseline lattice structure for each printing configuration. The sections highlighted green were selected because their components are likely to connect between layers. To print a perpendicular pattern, the second configuration should have similar characteristics, but the sections highlighted red did not.

Tests to determine rod rotation, based on data from the previous study [22] were done with concentric patterns in the same direction for the second configuration, allowing the first configuration to operate without any rotation. The rotation ratio was adjusted in increments and cross sections shown in **Figure 4** were analyzed. From these tests and the known baseline for the other configuration, mixing parameters for each of the primary print directions were selected and are shown in **Table 1** – Mixing parameter selection for specimens printed in this study **Table 1**. Additionally, because both operate at  $0^\circ$  and  $+90^\circ$  from the  $+X$  axis, the designed print extrusions could be printed with the same infill angles.

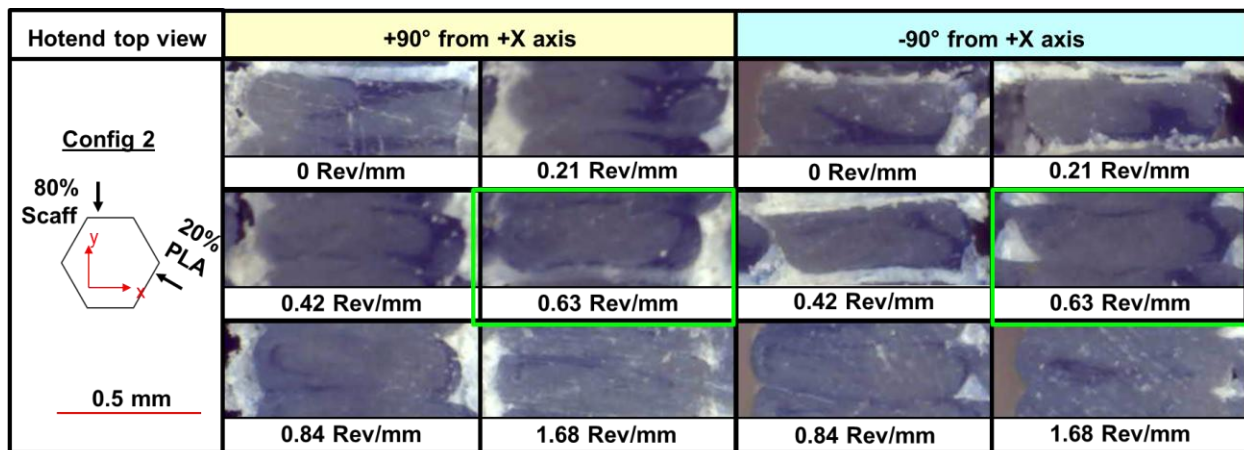


**Figure 4** – Investigation of extrusions for configuration 2 in the desired print directions. The rod was spun at a proportional rate of revolution to the extrusion of material. The extrusions highlighted in green contain characteristics desirable for building the lattice structure of this study.

**Table 1** – Mixing parameter selection for specimens printed in this study

	Configuration	Soluble Inlet	PLA Inlet	Rod Rotation	Minimum PLA	Extrusion Height	Extrusion Width
		Angle	Angle	rev/mm	%	mm	mm
Primary X Print Direction	1	+90	-150	0	35	0.2	0.8
Primary Y Print Direction	2	+90	-30	0.63	35	0.2	0.8

## Specimen post-processing

All the tensile specimens underwent post-processing to remove excess printed stock and prepare for testing. The printed stock sheets were given a template, **Figure 5-A**, to aid a user in applying a rotating blade to remove most of the material, which was then sanded to parallel edges **Figure 5-B**. At this point, a solid structure would be considered complete. For a specimen that required removal of soluble material, electrical tape was applied to the grip section of the specimen to minimize material washout and provide a more solid grip area **Figure 5-C** than the test region. Soluble material was removed by submersion in water and sonication at room temperature for approximately 6 hours, with occasional changing of the water to aid in dissolution of soluble material **Figure 5-D**. The specimen was then dried at 40° C in an oven with desiccant for 10 hours to remove moisture. Tape was then removed, and the specimen was considered ready for tensile testing **Figure 5-E**. The x-ray specimen was processed the same way but was not taped because no section needed protecting. The full PLA test specimen was not washed or dried.

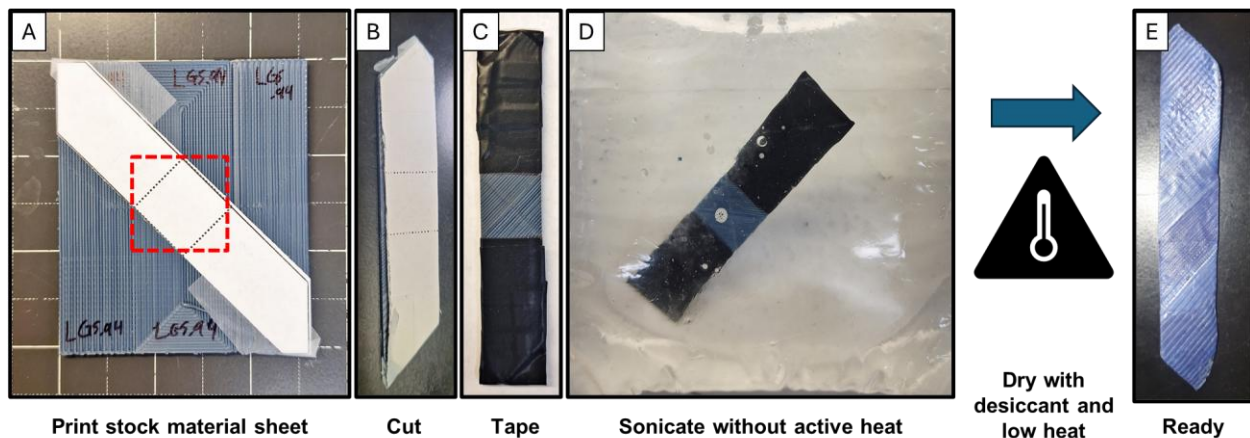


Figure 5 – Post processing steps for a printed stock sheet

## Optical and x-ray imaging

Optical imaging of specimens was performed with a Dino-Lite Edge PLUS microscope (Dunwell Tech Inc, United States of America). The uCT x-ray scan was performed on a SKYSCAN 1276 (Bruker Corporation, Massachusetts, United States of America). The specimen scanned was printed with a prescribed uniform mix ratio of 50% PLA and was post processed as described above. Images captured were with 4  $\mu\text{m}$  resolution at 50 kV, 2000  $\mu\text{A}$ , and no filter. Every image was captured at 0.2 degrees of rotation and a 2-frame averaging. The specimen was sandwiched in between foam to hold its position during the scan process.

Processing of the scan was performed using Dragonfly 3D World 2024 (Comet Technologies Canada Inc., Montreal, Canada). Thresholding was performed to filter out the mount and foam. The remaining voxels were segmented using a watershed technique to separate into groups of voxels based on the size of the group and how well they were interconnected. The intensity values for PLA and the soluble material were too close to differentiate between them. Any remaining groups that were believed to be the foam or mount after thresholding and

watershed were manually removed. The thresholding and final manual cleanup were done by visual analysis of the data and the corresponding physical specimen.

### **Tensile testing**

Specimens representing a range of PLA volume fractions were printed: 35, 50, 65, and 100% PLA. The remaining volume fraction of each was soluble material that was removed during the post-processing steps. Additionally, a functionally graded (FG) specimen was printed with extrusions ranging from 35% PLA at the center of the concentric pattern to 65% PLA at the edge of the region of interest in 2% increments, resulting in an average of 43% PLA in the test region, even though the region of interest has an average of 50% PLA as highlighted in **Figure 2**. For a point of reference, a 35% PLA specimen that had not been washed was tested to compare a solid printed structure against a solid structure of PLA.

Tensile testing was performed on an ADMET tensile tester (ADMET Inc., Norwood, MA). Specimens were mounted in pneumatic grips positioned 1" apart from each other, centering the specimen in all directions so that the test section is in the middle of the grips. Tests were performed at 1 mm/min until a loss of load. The cross-sectional area of each specimen was recorded as the product of the width and thickness at the center of the test region. No extensometer was used due to the difficult nature of mounting to a lattice, so displacement of the grips was used for analysis.

## **Results**

### **Observations of technique**

During the processing of the tensile specimens several potential defects were identified which are the result of the fabrication process and post-processing techniques. Along the centerline of each concentric pattern, where the final two extrusions are laid, overlap and overflow of the extrusion changes the beam shape and could be a potential disconnect between layers of the lattice system, as shown in **Figure 6-A**. Additionally, during the post-processing of the specimens a twist was found to appear in all of them in the same direction that the electrical tape was wrapped around the grip sections, **Figure 6-B**. Despite not adding heat, temperatures above 40° C were observed in the sonication bath which may have allowed for warping when under tension. The grip sections also appeared more compressed than their test section, **Figure 6-C**. On specimens with a low target PLA percentage, tape removal also removed extrusions from the grip section, **Figure 6-D**. Though the grip sections appeared to have a solid structure that was not removed during sonication, the pneumatic grips squeezing the grip sections resulted in soluble residue leaking from the grip section during the test, **Figure 6-E**. The pneumatic grips compensated for this change in dimension and prevented slipping.

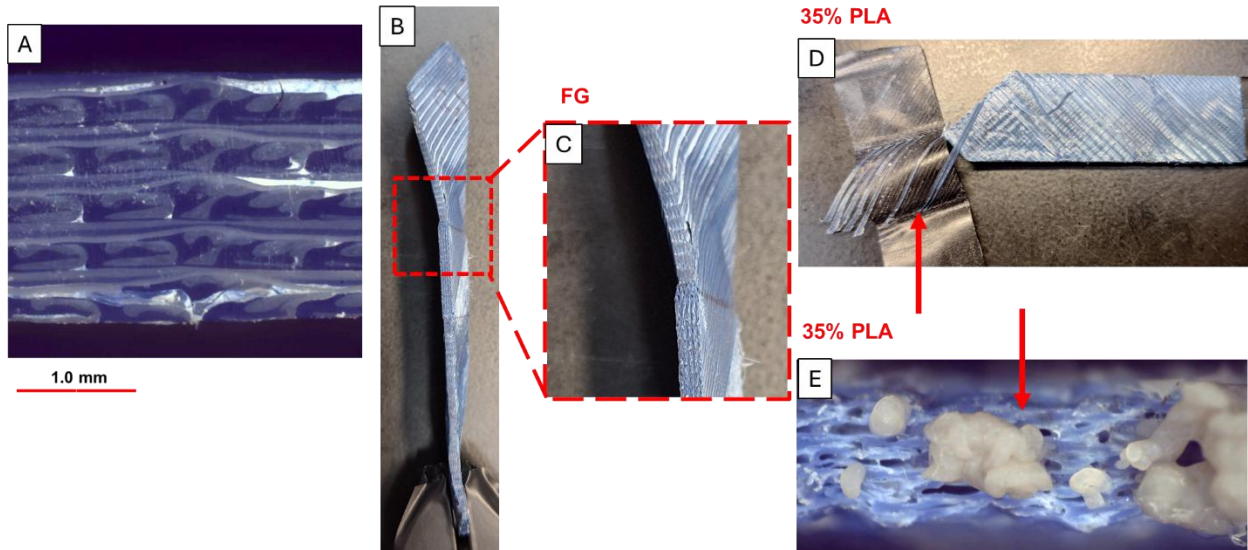


**Figure 6** – Observed defects on different printed tensile specimens (A) and as a result of the washing process (B-E)

The uCT scans provided direct measurement of the lattice structure’s geometry including dimensions of the beams. As shown in **Figure 7**, a representative region of the scan was analyzed for void content. Without inclusion of the largest single connected volume, 0.4% of voxels were not identified as the PLA beams. When that single connected volume, believed to be the void of the lattice structure, is included the content rises to 37.1% of voxels. This is below the predicted 50% of void that was prescribed on this specimen. Additionally, the beams have imperfections that may indicate the influence of flow on the internal geometry of the extrusions, as highlighted in the representative slices in **Figure 8**. Many beams contain large volumes of PLA extending into the middle of the void space.

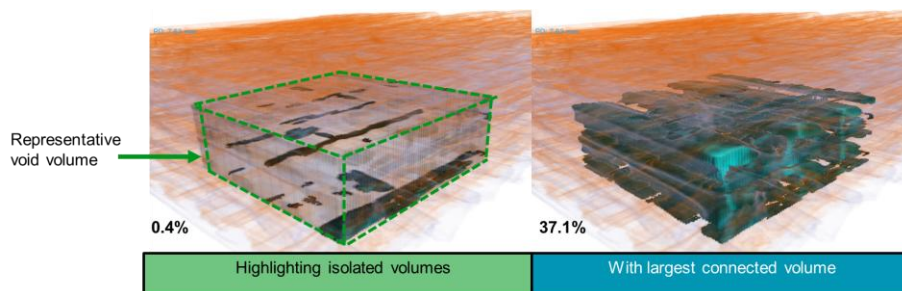


**Figure 7** – Analysis of representative region of the uCT specimen with void volumes highlighted. The isolated void volumes were not a part of the main group of voxels determined to be void content.

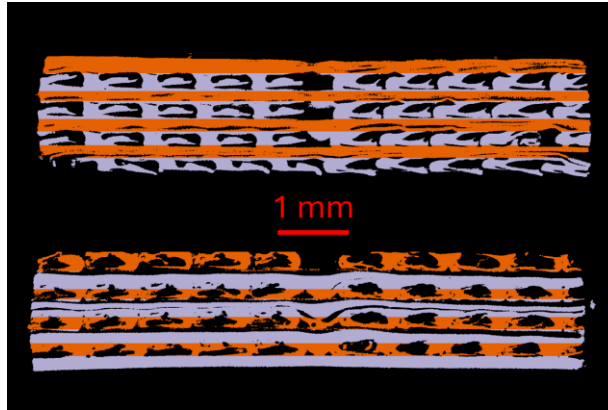


**Figure 8** – Cross section slices of the entire uCT scan, highlight the lattice beams in the Primary X and Primary Y orientations, colored here as purple and orange to help with visualization of layers and directions.

### Tensile characterization of lattices

Fractured tensile specimens are shown in **Figure 9**. All compositions except the 100% PLA solid structure fractured along one or both diagonals. The solid PLA structure fractured at the grips while the FG specimen had a variation in its fracture pattern including extrusions that extend past the main fracture line on alternate layers. The fractures which split through the diagonal of the lattice structure are very similar to the noted failure characteristics seen in [10] but may be caused by the noted defect at the centerline of the concentric print pattern. Observation of different specimens' fracture surfaces with the microscope are shown in **Figure 10**. In the FG specimen, the beams further from the center of the structure with higher PLA volume fraction were less deformed. At locations of lower PLA volume fraction, fibrils were observed suggesting high ductility. The 100% PLA specimen shows signs of brittle fracture throughout the fracture surface, while lower ratios of PLA have high amounts of crazing in alternating layers where the beams were broken during the test. The beams parallel to the fracture line demonstrate notably less damage and crazing. In the 35% PLA specimen, layers delaminated between layers is clear, as deformation of the beams due to transverse strain further separating the beams.

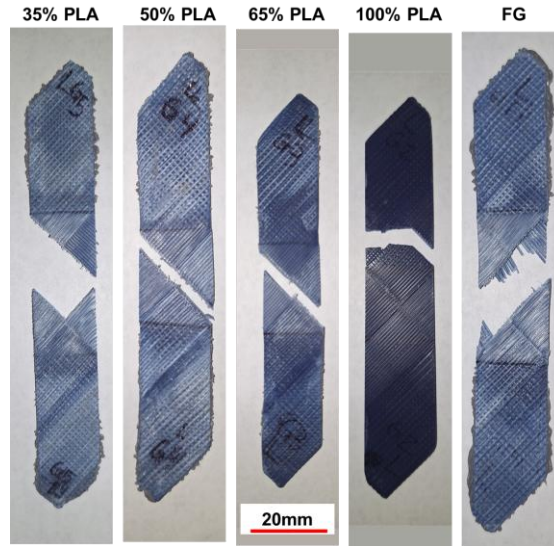


**Figure 9** – Tensile specimens after testing procedures. The scale applies to all images, though a fish-eye effect has caused distortion of their apparent size.

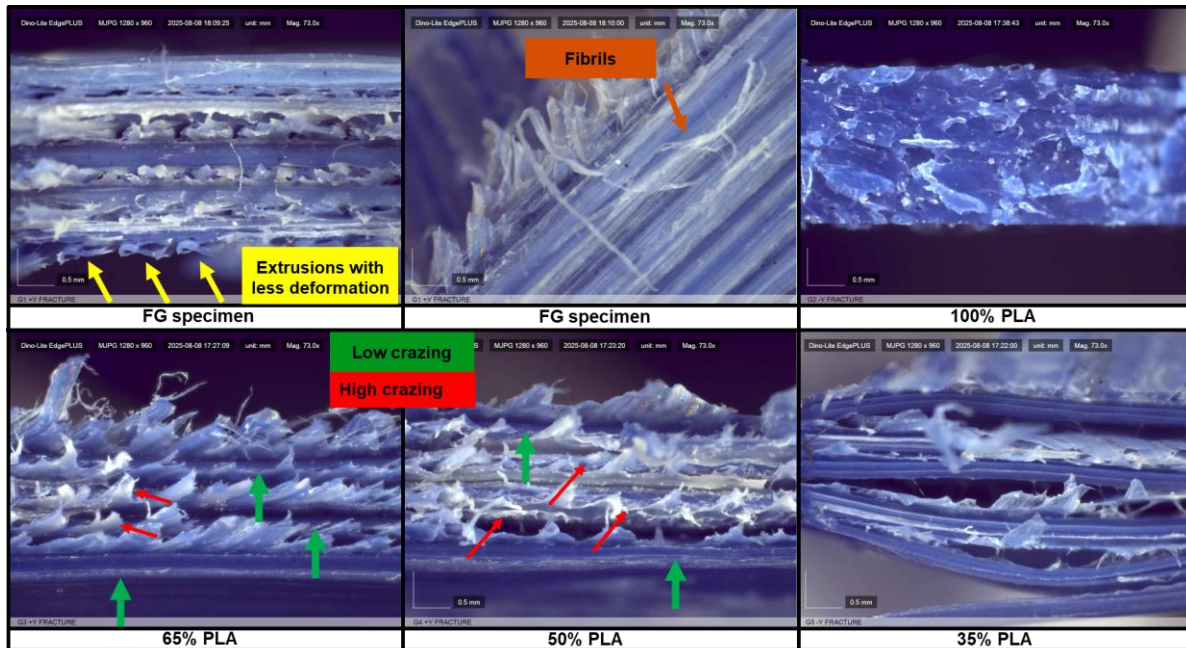


**Figure 10** – Fracture surfaces of specimens after tensile testing

The stress-deformation curves of the tensile tests are shown in **Figure 11**, and **Figure 12** shows the relationships between prescribed relative PLA density and tensile properties, normalized to the uniform lattice structures. The unwashed 35% PLA structure behaves very similar to the 100% PLA structure, meaning that before washing the specimens are expected to behave much like a solid structure just composed of two different materials. The lower ultimate tensile strength (UTS) of the unwashed 35% PLA is likely due to the weaker tensile performance of the soluble material. A relationship between reduced PLA content and reduced stiffness is noted, and the FG specimen with an estimated average of 43% PLA volume fraction in the test area has a stiffness between the 35% and 50% PLA specimens. However, the maximum

displacement of the FG specimen is larger than that of any of its comparative tests. Overall, the relationship between relative PLA density and stiffness is almost linear, while UTS and maximum displacement demonstrate non-linearly related to the nominal composition.

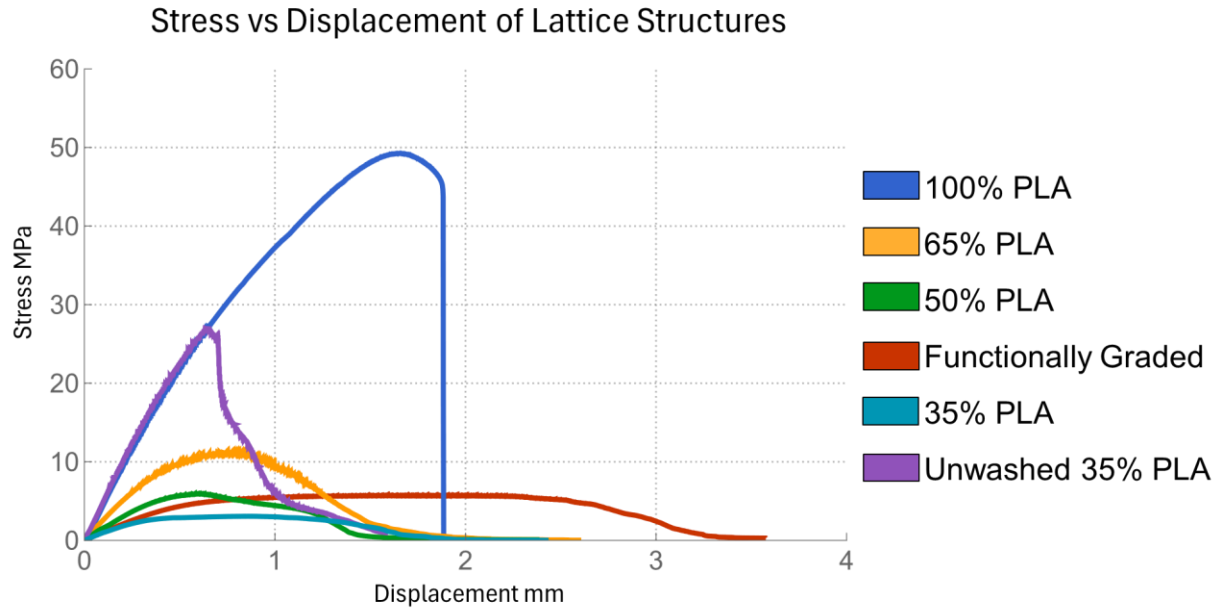


**Figure 11** – Tensile plots of the lattice structures. The functionally graded specimen has approximately 43% PLA in its testing section. The unwashed 35% PLA did not have the final post processing steps done to it.

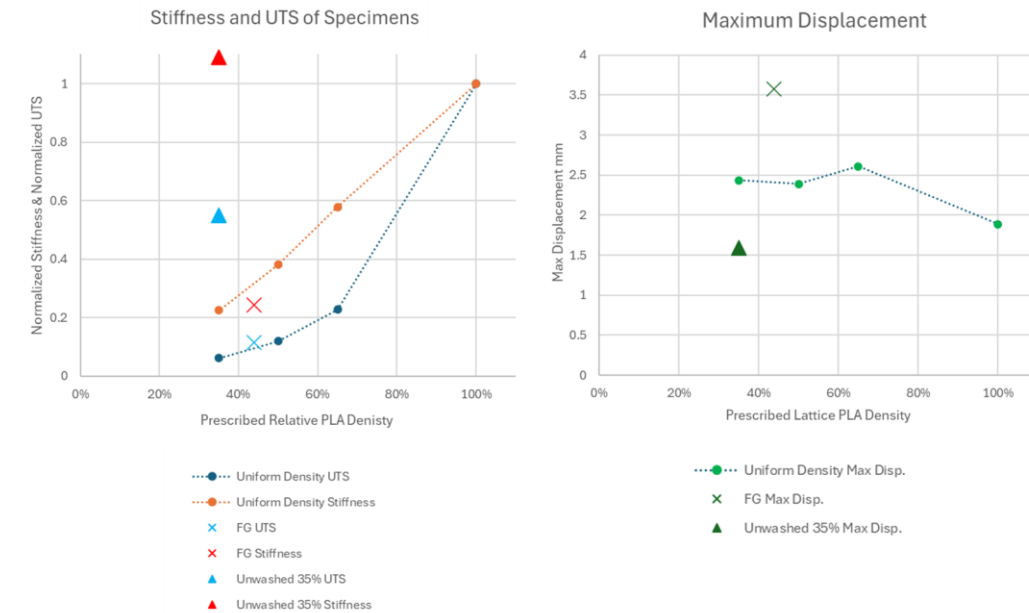


**Figure 12** – Comparison of lattice tensile properties as relative densities change

## Discussion

Through coextrusion of soluble and insoluble material, lattice structures which contain features smaller than the extrusion were printed using AFMF. To control the distribution of the

volume fraction of the insoluble structure in perpendicular print directions a rod was used to induce shear flow inside the hotend. In other implementations of sub-extrusion distribution control may be used such as physically changing the position of inlets during printing. This may reduce the effect of shear mixing and provide a simpler method for computing positional control regardless of extrusion orientation. Other variables not directly considered in this study likely impact the level of control that may be achieved, including the printing compatibility of the chosen materials, their relative viscosities and volume fraction while printing, and external flow conditions such as neighboring extrusions.

In the context of what was achieved here, tensile performance may be adjusted through relative solid structure density in the lattice, within a minimum amount of material to achieve a connected lattice system. While adjustments to the relative density provide control over stiffness, the use of a functional gradient of beam width and length through local variations of the relative density showed potential for increasing the maximum deformation of a structure. As the uCT data revealed, not all of the remaining solid material was contributing directly to the lattice beams as the mixing action redistributed it through the volume of extrusion. Additionally, the computed void content could be interpreted to indicate voids which are not well connected as part of the lattice and less void than was prescribed.

Though this study demonstrates lattice structures, the applications for a post-processing procedure to remove specific elements of a print are not limited to this case. Common defects in AM and FFF may be mitigated this way such as stair stepping on angled surfaces or over-extrusion where infill percentages are high. Where there is no room for an additional extrusion to create a smooth surface in these positions, a smaller nozzle could potentially be used which adds time and complexity to the print process. Alternatively, a full extrusion is added which contains only a partial amount of structural material placed where needed. Removal of soluble materials then offers improved surface quality. Additionally, applications where reduction of time or an increase of printability require a larger nozzle size such as large format AM could benefit from this technique to improve the resolution of detail they can print. Support structure interfaces can additionally be contained in the support structure itself as part of the extrusions neighboring the part and porous structures may be made in a controlled manner by printing solid and removing the soluble material.

## **Conclusions**

Lattice structures offer the benefit of unique responses to load conditions and may be tailored to their application and fabrication method. Additive manufacturing of lattices with fused filament fabrication was limited to the resolution offered by a single extrusion to control the width and length of the lattice beams. This study suggests a method for printing lattices with sub-extrusion beam dimensions through controlled co-extrusion of soluble and insoluble material and post-processing. Distribution of material inside an extrusion is dependent on the orientation of the extrusion and a form of control is required to achieve consistent geometry through a print, achieved here through the use of shear flow induced by an active mixing rod. Analysis of the method with micro computed tomography revealed that the lattice structure is achievable but may be improved on. Simple lattice structures with uniform or functionally graded beam

dimensions were fabricated and tensile tested to demonstrate the capabilities offered by this technique in achieving micro lattices and the large change in response, especially maximum deformation, while maintaining relative stiffness. Manufacturing technologies built for these express purposes combined with software to control these distributions could have the potential to greatly improve the resolution of and reduce defects in printed parts.

### **Acknowledgements**

The authors would like to thank students at The University of Texas at El Paso, including Daniel Hernandez and Davina Carrera for their help in completing this work. Imaging was performed at the Imaging & Behavioral Neuroscience (IBN) Facility Imaging Core at The University of Texas at El Paso, supported by the College of Science and the Office of Research & Innovation. The IBN Facility was supported by the Office of the Director, National Institutes of Health (NIH), under award number C06OD032074. We thank Sivasai Balivada for his assistance. The content is solely the responsibility of the authors and does not necessarily represent the official views of the NIH. Parts of this research were conducted using Dragonfly 3D World, provided by Comet Technologies Canada Inc., Montreal, Canada.

### **Conflict of Interest**

The University of Texas System board of regents has patents for technologies described in this work for which Ian A. Rybak, Joseph W. McKee, and Joshua T. Green are inventors.

### **References**

- [1] E. MacDonald and R. Wicker, "Multiprocess 3D printing for increasing component functionality," *Science*, vol. 353, no. 6307, p. aaf2093, Sept. 2016, doi: 10.1126/science.aaf2093.
- [2] Y. Tang, G. Dong, Q. Zhou, and Y. F. Zhao, "Lattice Structure Design and Optimization With Additive Manufacturing Constraints," *IEEE Trans. Autom. Sci. Eng.*, vol. 15, no. 4, pp. 1546–1562, Oct. 2018, doi: 10.1109/TASE.2017.2685643.
- [3] A. Kumar, L. Collini, A. Daurel, and J.-Y. Jeng, "Design and additive manufacturing of closed cells from supportless lattice structure," *Addit. Manuf.*, vol. 33, p. 101168, May 2020, doi: 10.1016/j.addma.2020.101168.
- [4] C. Beyer and D. Figueroa, "Design and Analysis of Lattice Structures for Additive Manufacturing," *J. Manuf. Sci. Eng.*, vol. 138, no. 121014, Sept. 2016, doi: 10.1115/1.4033957.
- [5] D. G. Zisopol, M. Minescu, and D. V. Iacob, "A Study on the Evaluation of the Compression Behavior of PLA Lattice Structures Manufactured by FDM," *Eng. Technol. Appl. Sci. Res.*, vol. 13, no. 5, pp. 11801–11806, Oct. 2023, doi: 10.48084/etasr.6262.
- [6] K. Ushijima, W. J. Cantwell, and D. H. Chen, "Prediction of the mechanical properties of micro-lattice structures subjected to multi-axial loading," *Int. J. Mech. Sci.*, vol. 68, pp. 47–55, Mar. 2013, doi: 10.1016/j.ijmecsci.2012.12.017.

- [7] G. Dong, Y. Tang, and Y. F. Zhao, “A Survey of Modeling of Lattice Structures Fabricated by Additive Manufacturing,” *J. Mech. Des.*, vol. 139, no. 100906, Aug. 2017, doi: 10.1115/1.4037305.
- [8] C. Casavola, A. Cazzato, V. Moramarco, and C. Pappalettere, “Orthotropic mechanical properties of fused deposition modelling parts described by classical laminate theory,” *Mater. Des.*, vol. 90, pp. 453–458, Jan. 2016, doi: 10.1016/j.matdes.2015.11.009.
- [9] W. Tao and M. C. Leu, “Design of lattice structure for additive manufacturing,” in *2016 International Symposium on Flexible Automation (ISFA)*, Aug. 2016, pp. 325–332. doi: 10.1109/ISFA.2016.7790182.
- [10] Y. Wu and L. Yang, “The effect of unit cell size and topology on tensile failure behavior of 2D lattice structures,” *Int. J. Mech. Sci.*, vol. 170, p. 105342, Mar. 2020, doi: 10.1016/j.ijmecsci.2019.105342.
- [11] Y. Han and W. F. Lu, “A Novel Design Method for Nonuniform Lattice Structures Based on Topology Optimization,” *J. Mech. Des.*, vol. 140, no. 091403, July 2018, doi: 10.1115/1.4040546.
- [12] I. B. Ishak and P. Larochelle, “MotoMaker: a robot FDM platform for multi-plane and 3D lattice structure printing,” *Mech. Based Des. Struct. Mach.*, vol. 47, no. 6, pp. 703–720, Nov. 2019, doi: 10.1080/15397734.2019.1615943.
- [13] J. Nguyen, S. Park, and D. Rosen, “Heuristic optimization method for cellular structure design of light weight components,” *Int. J. Precis. Eng. Manuf.*, vol. 14, no. 6, pp. 1071–1078, June 2013, doi: 10.1007/s12541-013-0144-5.
- [14] J. Xiong *et al.*, “Advanced Micro-Lattice Materials,” *Adv. Eng. Mater.*, vol. 17, no. 9, pp. 1253–1264, 2015, doi: 10.1002/adem.201400471.
- [15] Z. Liu, M. A. Meyers, Z. Zhang, and R. O. Ritchie, “Functional gradients and heterogeneities in biological materials: Design principles, functions, and bioinspired applications,” *Prog. Mater. Sci.*, vol. 88, pp. 467–498, July 2017, doi: 10.1016/j.pmatsci.2017.04.013.
- [16] I. M. El-Galy, B. I. Saleh, and M. H. Ahmed, “Functionally graded materials classifications and development trends from industrial point of view,” *SN Appl. Sci.*, vol. 1, no. 11, p. 1378, Oct. 2019, doi: 10.1007/s42452-019-1413-4.
- [17] B. A. Moreno-Núñez, C. D. Trevino-Quintanilla, J. C. Esponiza-Garcia, E. Uribe-Lam, and E. Cuan-Urquizo, “Effect of Printing Parameters on the Internal Geometry of Products Manufactured by Fused Filament Fabrication (FFF),” 2023, Accessed: Sept. 02, 2025. [Online]. Available: <https://hdl.handle.net/2152/124478>
- [18] S. A. Yadlapati, “Influence of FDM Build Parameters on Tensile and Compression Behaviors of 3D Printed Polymer Lattice Structures”.
- [19] J. T. Green *et al.*, “Local composition control using an active-mixing hotend in fused filament fabrication,” *Addit. Manuf. Lett.*, vol. 7, p. 100177, Dec. 2023, doi: 10.1016/j.addlet.2023.100177.
- [20] T. Teng, Y. Zhi, and M. Akbarzadeh, “Single-Nozzle Multi-Filament System with Active Mixing for High-Fidelity Multimaterial Additive Manufacturing,” 2024, *SSRN*. doi: 10.2139/ssrn.4773564.
- [21] R. G. Lahaie, C. J. Hansen, and D. O. Kazmer, “Development of Fused Deposition Modeling of Multiple Materials (FD3M) Through Dynamic Coaxial Extrusion,” *3D Print. Addit. Manuf.*, vol. 11, no. 2, pp. 485–495, Apr. 2024, doi: 10.1089/3dp.2022.0197.

- [22] I. A. Rybak, D. L. Hernandez, R. V. Gonzalez, and J. T. Green, "Controlled Distribution of Composition within Extrusions as Enabled by an Active-Mixing Hotend," 2024, Accessed: Sept. 05, 2025. [Online]. Available: <https://hdl.handle.net/2152/130816>
- [23] L. M. Galantucci, F. Lavecchia, and G. Percoco, "Experimental study aiming to enhance the surface finish of fused deposition modeled parts," *CIRP Ann.*, vol. 58, no. 1, pp. 189–192, Jan. 2009, doi: 10.1016/j.cirp.2009.03.071.
- [24] J. Žigon, M. Kariž, and M. Pavlič, "Surface Finishing of 3D-Printed Polymers with Selected Coatings," *Polymers*, vol. 12, no. 12, p. 2797, Dec. 2020, doi: 10.3390/polym12122797.
- [25] J. T. Green, "A New Approach To Multiplanar, Real-Time Simulation Of Physiological Knee Loads And Synthetic Knee Components Augmented By Local Composition Control In Fused Filament Fabrication".
- [26] E. Cuan-Urquizo, E. Barocio, V. Tejada-Ortigoza, R. B. Pipes, C. A. Rodriguez, and A. Roman-Flores, "Characterization of the Mechanical Properties of FFF Structures and Materials: A Review on the Experimental, Computational and Theoretical Approaches," *Materials*, vol. 12, no. 6, p. 895, Jan. 2019, doi: 10.3390/ma12060895.
- [27] D. Croccolo, M. De Agostinis, and G. Olmi, "Experimental characterization and analytical modelling of the mechanical behaviour of fused deposition processed parts made of ABS-M30," *Comput. Mater. Sci.*, vol. 79, pp. 506–518, Nov. 2013, doi: 10.1016/j.commatsci.2013.06.041.